International Journal for Innovative Engineering and Management Research
A Peer Revieved Open Access International Journal
www.ijiemr.org

COPY RIGHT

ELSEVIER
SSRN

IJIEMR Transactions, online available on 14th Dec 2018. Link
:http://www.ijiemr.org/downloads.php?vol=Volume-07&issue=ISSUE-13

Title: BI-DIRECTIONAL SINGLE STAGE MULTILEVEL INVERTER FED INDUCTION MOTOR DRIVE FOR BATTERY ENERGY STORAGE SYSTEM

Volume 07, Issue 13, Pages: 412–425.

Paper Authors

B.UMA MAHESWARI, G.SANDHYA SREE.

Gonna Institute of Information Technology & Sciences, Vizag, A.P, India

USE THIS BARCODE TO ACCESS YOUR ONLINE PAPER

To Secure Your Paper As Per UGC Guidelines We Are Providing A Electronic Bar Code

International Journal for Innovative Engineering and Management Research
PEER REVIEWED OPEN ACCESS INTERNATIONAL JOURNAL
www.ijiemr.org

BI-DIRECTIONAL SINGLE STAGE MULTILEVEL INVERTER FED INDUCTION MOTOR DRIVE FOR BATTERY ENERGY STORAGE SYSTEM

B.UMA MAHESWARI[1], G.SANDHYA SREE[2].
[1]M.Tech Student Scholar, Dept of EEE, Gonna Institute of Information Technology & Sciences, Vizag, A.P, India
[2]Assistant Professor, Dept of EEE, Gonna Institute of Information Technology & Sciences, Vizag, A.P, India

ABSTRACT- In this paper presents Bi-Directional single stage grid connected inverter for battery energy storage system. The proposed BGS is consists of Multiple bi-directional Buck boost DC-DC converters and a DC-AC inverter. Individual power control for each battery, single stage power conversion, pulsating charge/discharge currents and low battery & DC bus voltages are the advantages of the proposed topology. By using the proposed BSG, increases the Lifetime and flexibility of the battery energy storage system and also the power flow of the battery is controlled without the need of current sensors. The current ripple of output inductor can be reduced by the interleaved operation between Bi-directional Buck-boost converter operations. Photovoltaic system is fed to the Proposed BSG Inverter to run the MLI fed Induction Motor. Matlab/Simulink based simulation model is developed and the performance of the proposed topology is analysed.

Keywords: Battery Energy Storage system, multilevel inverter, Grid connection Inverter, Induction motor

I. INTRODUCTION

Because of the fossil fuel exhaustion and global warming issue, renewable energies such as the photovoltaic (PV) power and wind turbines are more and more popular recently. However, the fluctuations of the high penetration renewable energy will cause the negative impact to the grid voltage and frequency stabilization. A battery energy storage system is a promising candidate to increase the penetration rate of the renewable energy. For the microgrid application, the battery energy storage system is essential not only for controlling and managing the energy of distributed generation units such as PVs, wind turbines, and microturbines for the stability of the power system, but also for protecting loads from grid fault conditions. As shown in Fig.1, the conventional battery energy storage system consists of a battery array, which is formed by many battery Modules connected in series or parallel, and a bidirectional grid-tied dc–ac inverter as a full-bridge inverter. Circuit simplicity is the main advantage of this type of battery energy storage system but the total power capacity may be easily reduced by a particular overcharging/discharging battery module due to the battery tolerance, unequal battery losses, and so on. In order to maximize energy storage, the voltage of the individual battery module connected in series to form a dc bus as the input of the grid-tied inverter must be equalized with each other. The general solution to solve the battery capacity reduction problem is to use extra balancing circuit to connect each battery module and balance the

International Journal for Innovative Engineering and Management Research
PEER REVIEWED OPEN ACCESS INTERNATIONAL JOURNAL
www.ijiemr.org

charge of all battery modules. However, the balancing circuit may result in the reduction of total efficiency and the increase of cost and circuit complexity.

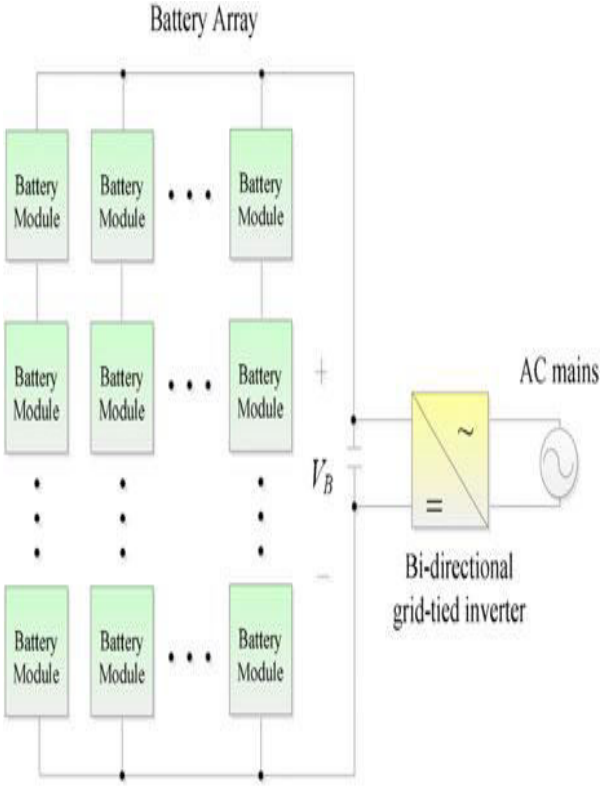

Fig.1.Conventional Battery Energy Storage System

Instead of using balancing circuit, Fig.2 shows the different configuration of the grid-tied battery energy storage system to balance the charge of all battery modules. A two-stage configuration to step up the voltage by a dc–dc converter and transfer the dc power into ac power by a dc–ac inverter is shown in Fig.2 (a). Because of the parallel connection of each battery module, the equalization of battery modules can be naturally achieved. Also, the two-stage configuration implies a simpler system design with lower control complexity. However, the high current stress of the dc–dc converter and an inverter as the second stage will reduce the overall conversion efficiency. Thus, the power capacity of this type of configuration is limited due to the efficiency and the current stress considerations. An alternative configuration for the battery energy storage system is to adopt a dc–ac micro inverter for each battery module as shown in Fig.2(b).Compared to the two-stage configuration, the micro inverter offers more flexibility and fault tolerance in the battery energy storage system. Since each battery module has its own grid-connected micro inverter, the output power of the battery module can be individually controlled in despite of other battery module mismatching. However, many challenges still remain in the way of achieving lower cost and higher conversion efficiency. Fig.2(c) shows the cascade-type configuration for the battery energy storage system where the output terminals of the inverter are connected in series. Since low voltage rating components can be adopted with single-stage conversion, the inverter efficiency and cost can be improved. However, the control of those series-connected dc–ac inverters is complicated and the reliability of the battery storage system may be reduced.Another key issue of the battery energy storage system is the life-time of the battery modules. Based on the power density and battery life consideration, the lead-acid battery and Li-ion battery are the most commonly used energy storage component for the battery energy storage system. However, the degradation of the electrochemical battery will affect the system's reliability dramatically. It has been reported that the sinusoidal current can improve the Li battery charging efficiency by comparing to the conventional constant-current constant voltage charging strategy. Also, using pulsating currents to charge/discharge the electrochemical battery can improve the battery efficiency as well as increase the life-time of the battery.Conventionally, the battery energy storage system needs the two-stage converter to achieve the dc–ac function for the grid-connected inverter and to produce the

International Journal for Innovative Engineering and Management Research
PEER REVIEWED OPEN ACCESS INTERNATIONAL JOURNAL
www.ijiemr.org

pulsating charging/discharging current for the battery. Unfortunately, it will reduce the power conversion efficiency of the precious energy storage. Moreover, expensive current sensors are required to calculate the battery module output power for the output power control. Both the two-stage configuration and the expensive current sensor become the major barriers for the battery energy storage system. Therefore, a novel bidirectional single-stage grid-connected inverter (BSG inverter) without using current sensors, as shown in Fig. 3, is proposed.

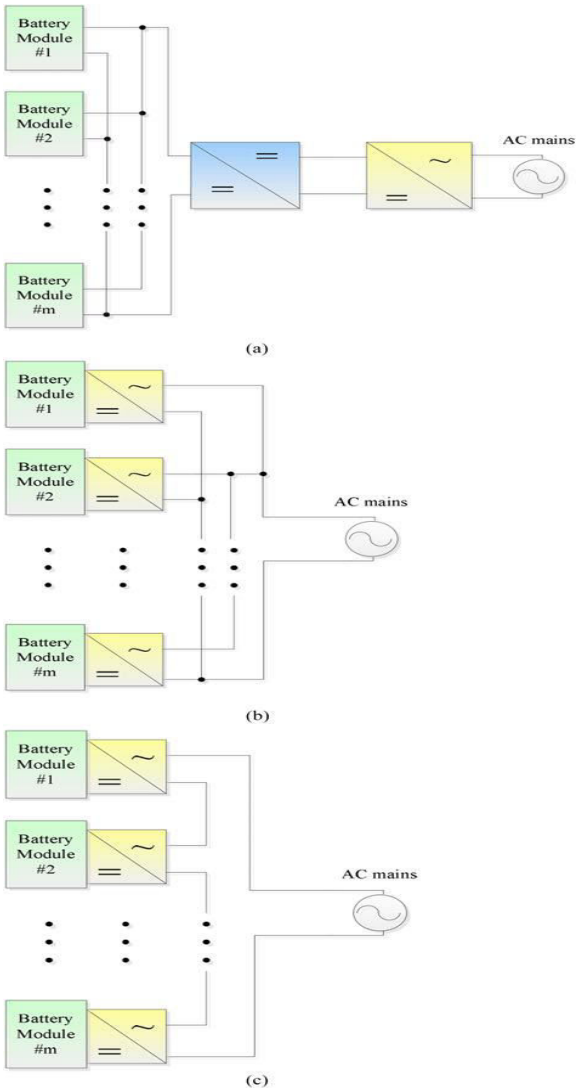

Fig.2. Different configuration of the battery energy storage system.(a) Two-stage configuration. (b) Micro inverter configuration.(c) Cascade-type configuration.

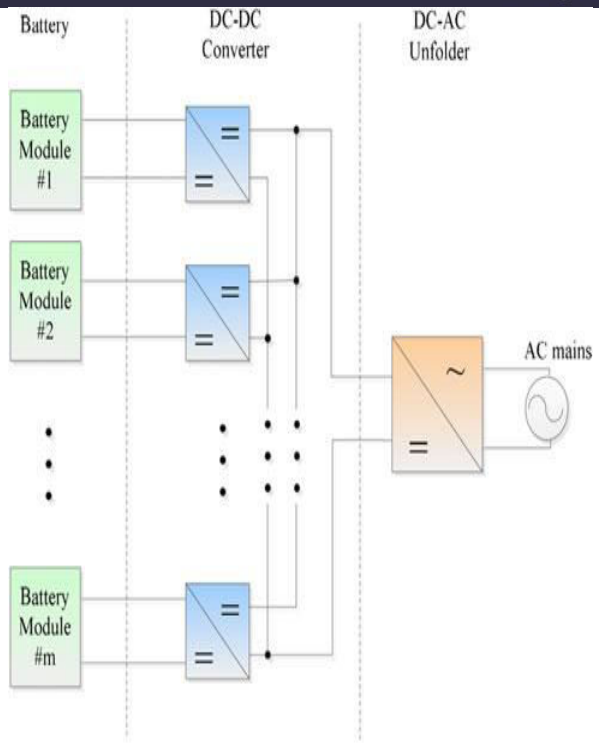

Fig.3 Proposed BSG-inverter for the battery energy storage system

In Fig. 3, each battery module has its own dc–dc converter to control the output power while the dc–ac unfolder is realized by an output inductor and four active switches operated at ac line frequency. The dc–dc converter produces a high frequency pulsating dc current with a sinusoidal envelope. Therefore, low battery and dc-bus voltages can be accomplished. The pulsating charging/discharging current can help to extend the battery module's lifetime, too. The dc–ac unfolder can convert the high frequency pulsating dc current generated by the dc–dc converters into a sinusoidal one with utility line frequency. Because the unfolder only switches at the zero crossing of the line voltage, its switching loss can be neglected by comparing to those power switches in the dc–dc converter. Therefore, the energy of each battery module is transferred to the ac mains by means of single-stage power conversion. Because of the single-stage operation, the power conversion efficiency can be improved. For the battery energy storage system, current

International Journal for Innovative Engineering and Management Research
PEER REVIEWED OPEN ACCESS INTERNATIONAL JOURNAL
www.ijiemr.org

sensors are always needed. Conventionally, two current sensors, one for the battery management system (BMS), which includes the state of charge and temperature monitoring, and the other for the power converter, which realizes the current control capability, are demanded for the battery energy storage system. The proposed BSG-inverter can achieve the desired power flow control without the need of current sensors. Also, it can be adopted for different BMSs as long as the communication protocol for the power flow command is determined.The proposed BSG-inverter can improve the power conversion efficiency, reduce the output inductor size, eliminate the input current sensor, and simplify the control circuit. Moreover, the proposed BSG-inverter can achieve individual power control of each battery module so that important features of battery equalization, capacity flexibility, and hot swapping can be accomplished. In this paper, the operation principle of the BSG-inverter will be introduced and the power flow control of each battery module without current sensor will be developed. Computer simulation and preliminarily experiments are shown to verify the performance of the proposed BSG-inverter.

II. PROPOSED BSG-INVERTER

The circuit diagram of the proposed BSG-inverter, which is composed of m sets of distributed buck–boost type dc–dc converters (BBCs) and a dc–ac unfolder, is shown in Fig.4. Each BBC consists of two switches, two diodes, and one inductor. It can convert the dc current generated by the battery module into a high frequency pulsating dc current. This high frequency pulsating output current of the BBCs will be converted into sinusoidal one with utility line frequency by the dc–ac unfolder of four active switches operated at low switching frequency and an LC filter. The proposed BSG-inverter will comply with the power commands, which is coming from the central control unit of the BMS, to charge or discharge the battery modules. The power flow from each battery module is transferred to the ac mains by means of single-stage power conversion. Also, the BBCs can be operated with interleaving to reduce the current ripple of the output inductor.

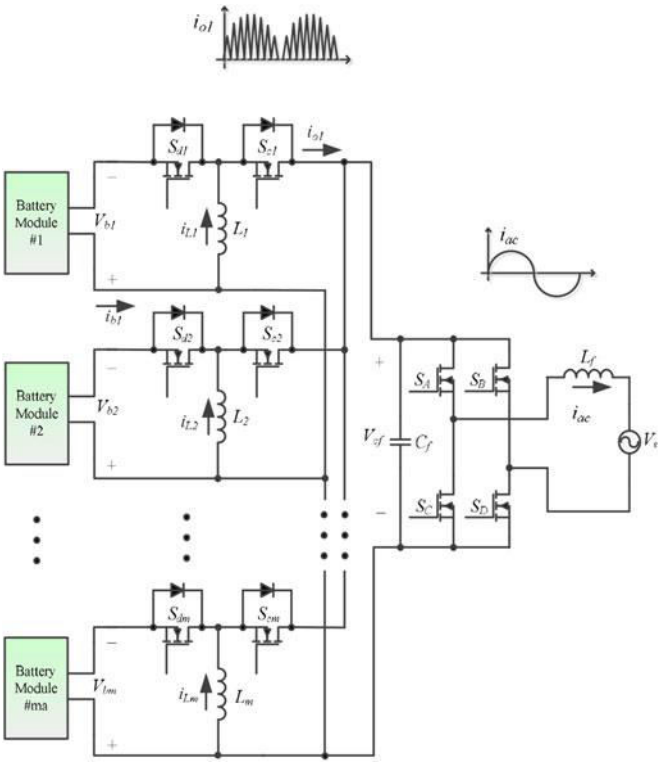

Fig.4 Circuit diagram of the proposed BSG-inverter.

(A) DISCHARGING MODE OPERATION

For battery discharging mode of the first BBC set in Fig.4, the switch S_{c1} is always turned off and the gate signal of S_{d1} can be generated by comparing the rectified sinusoidal signal V_{sin} with the saw-tooth carrier signal V_{saw} with discontinuous current mode (DCM) operation as shown in Fig.5 (a). Because of the rectified sinusoidal pulse width modulation (SPWM) control with DCM operation, the waveform of the inductor current, i_{L1}, has an envelope of the rectified ac mains. During the half-cycle of the grid line, the total switching numbers N can be expressed as follows:

$$N = fs/2f \quad (1)$$

International Journal for Innovative Engineering and Management Research
PEER REVIEWED OPEN ACCESS INTERNATIONAL JOURNAL
www.ijiemr.org

where fs is the switching frequency and f is the grid frequency. Typical waveforms of the inductor current, i_{L1}, and output current, i_{o1}, for the DCM operation during the k th switching cycle are shown in Fig.5(b).

In Fig.5(b), $i_{d\,p\,1}$ [k], $d_{d\,1}$ [k], and $d_{d\,2}$ [k] are defined as the peak current, the charging duty ratio, and the discharging duty ratio of the input inductor L_1 of the kth switching period T_s , respectively. For the first BBC set, during the charging period of the input inductor L_1 , the active switch $S_{d\,1}$ is turned on and the voltage potential across the input inductor L_1 is equal to the battery voltage $V_{b\,1}$ which results in the linearly increased inductor current. When the switch $S_{d\,1}$ is turned off, the voltage potential across the input inductor L_1 is reversed and equal to the capacitor voltage V_{cf} which can be assumed to be the rectified ac mains because of the dc–ac unfolder. Due to the DCM operation,

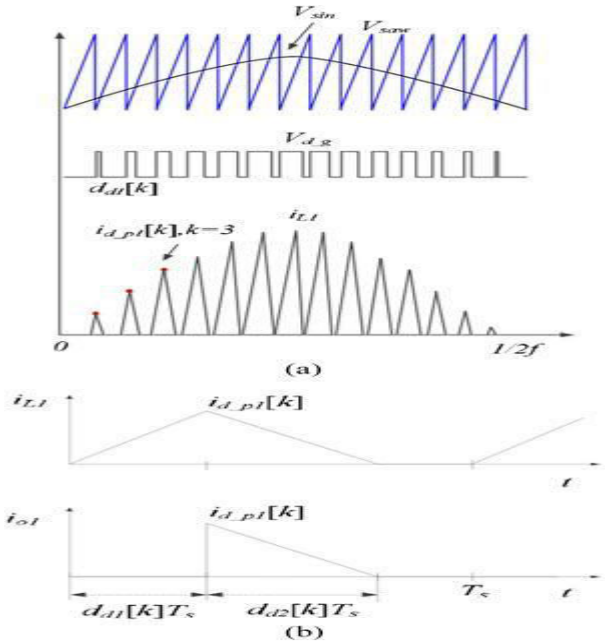

Fig.5. Control signal generation and input inductor current waveform of the first BBC in battery discharging mode. (a) Control signal generation.
(b) Typical input inductor current and output current waveforms of the first BBC during the kth switching cycle.

the inductor current $i_{L\ 1}$ decreases to zero during the discharging period of the input inductor L_1 . The peak current of the input inductor of the kth switching cycle can be expressed as follows:

$$i_{d\_p1}[k] = \frac{V_{b1}}{L_1} \cdot d_{d1}[k]T_s = \frac{V_{cf}[k]}{L_1} \cdot d_{d2}[k]T_s \qquad (2)$$

Where Vcf [k] is the output capacitor voltage during the kth switching cycle. Due to the DCM SPWM control, (2) can be further modified as follows:

$$i_{d\_p1}[k] = \frac{V_{b1}}{L_1 f_s} \cdot D_{p1} \sin\left(\frac{k\pi}{N}\right) \qquad (3)$$

Where $Dp1$ is the maximum duty ratio during the half-cycle of the grid line. To ensure the DCM operation in battery discharging mode, $Dp1$ must follow the following restriction:

$$D_{p1} < \left(\frac{\sqrt{2}V_{ac}}{V_{b1} + \sqrt{2}V_{ac}}\right) \qquad (4)$$

where Vac is the rms value of utility grid line voltage. It should be mentioned that the desired $Dp1$ can be easily obtained by controlling the amplitude of the rectified sinusoidal signal Vsin as shown in Fig.5(a). The average output current of the first BBC during the positive half-cycle can be derived as follows:

$$\langle i_{o1} \rangle = \frac{1}{N} \sum_{k=1}^{N} \frac{i_{d\_p1}[k] d_{d2}[k] T_s}{2}. \qquad (5)$$

From (2) and (5), the average value of the output impedance of BBC can be expressed as follows:

International Journal for Innovative Engineering and Management Research
PEER REVIEWED OPEN ACCESS INTERNATIONAL JOURNAL
www.ijiemr.org

$$\frac{\langle V_{cf}\rangle}{\langle i_{o1}\rangle} = \frac{1}{N}\sum_{k=1}^{N}\frac{2L_1V_{cf}^2[k]}{V_{b1}^2 d_{d1}^2[k]T_s^2}. \quad (6)$$

In (6), the ratio of *V*cf and *dd*1 for each *k*th switching cycle can be approximated as a constant since both of them can be approximated as rectified sinusoidal functions. It implies that the BBC has a constant output impedance and can inject power in to the ac mains with an almost unity power factor. Due to the DCM SPWM control with the current waveforms shown in Fig.5(b), the average battery discharging power can be obtained as follows:

$$P_{b1} = \frac{V_{b1}}{2N}\sum_{k=1}^{N} i_{d\_p1}[k]d_{d1}[k]. \quad (7)$$

Combining (2), (3), and (7), the expression of the average battery discharging power becomes

$$P_{b1} = \frac{f}{L_1 f_s^2}\sum_{k=1}^{N}\left(V_{b1}D_{p1}\cdot\sin\left(\frac{k\pi}{N}\right)\right)^2. \quad (8)$$

Eq. (8) reveals that the average discharging power is only related to *Vb*1 and *Dp*1 if other parameters (*f, fs*, *N*, and *L*1)are carefully designed. In other words, the battery discharging power can be determined without measuring the battery current. By measuring the battery voltage *Vb*1 to generating appropriate maximum duty ratio *Dp*1 of the BBC, it is possible to realize the individual power-handling capability required for the battery energy storage system. Also, (8) implies that the variation of inductance value will affect the accuracy of the output power. It is similar to the situation that an imprecise current sensor will lead to an inaccurate output current control. Hence, it is necessary to calibrate the power calculation and determine the effective inductor value after the hardware circuit is implemented.

(B) CHARGING MODE OPERATION

For battery charging mode of the first BBC set in Fig.4, the switch *Sd*1 is always turned off and the gate signal of *Sc*1 can be generated by comparing the reference signal *V*ref with the saw-tooth carrier signal *V*saw with DCM operation as shown in Fig.6(a). In Fig.6(b), *dc*1 is defined as the charging duty ratio of the input inductor *L*1 and *dc*2[*k*] is defined as the discharging duty ratio of the input inductor *L*1 of the *k*th switching period *Ts*. For the first BBC set, during the charging period of the input inductor *L*1, the active switch *Sc*1 is turned on and the voltage potential across the input inductor *L*1 is equal to the capacitor voltage *V*cf which can be assumed to be the rectified ac mains because of the dc–ac unfolder. When the switch *Sc*1 is turned off, the voltage potential across the input inductor *L*1 is reversed and equal to the battery voltage *Vb*1 which results in the linearly decreased inductor current. Due to the DCM operation, the inductor current *iL*1 decreases to zero during the discharging period. The peak current of the input inductor of the *k*th switching cycle can be expressed as follows:

$$i_{c\_p1}[k] = -\frac{V_{cf}[k]}{L_1}\cdot d_{c1}T_s = \frac{V_{b1}}{L_1}\cdot d_{c2}[k]T_s. \quad (9)$$

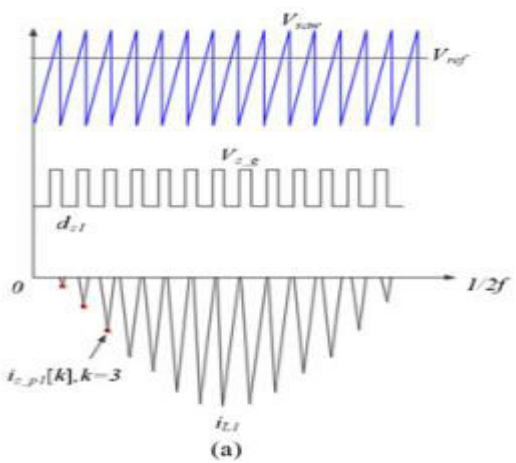

International Journal for Innovative Engineering and Management Research
PEER REVIEWED OPEN ACCESS INTERNATIONAL JOURNAL
www.ijiemr.org

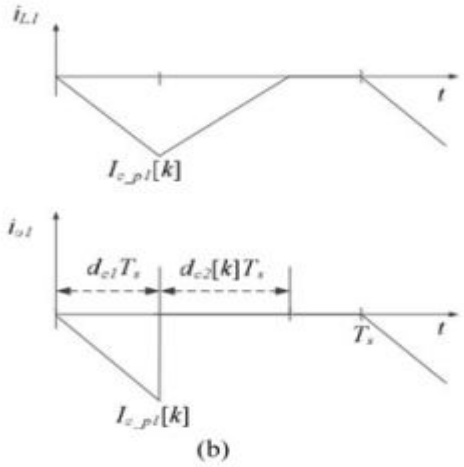

Fig. 6. Control signal generation and input inductor current waveform of the first BBC in battery charging mode.
(a) Control signal generation.
(b) Typical input inductor current and output current waveforms of the first BBC during the *k*th switching cycle.

Also, to ensure the DCM operation in battery charging mode, *dc*1 must follow the following restriction:

$$d_{c1} < \left(\frac{V_{b1}}{V_{b1} + \sqrt{2}V_{ac}} \right). \qquad (10)$$

Due to the DCM SPWM control with the current waveforms shown in Fig.6(b), the average battery charging power can be obtained as follows:

$$P_{b1} = \frac{f d_{c1}^2}{L_1 f_s^2} \sum_{k=1}^{N} (V_{cf}[k])^2. \qquad (11)$$

Equation (11) reveals that the average battery charging power is only related to *V*cf [*k*] and *dc*1 if other parameters (*fs*, *N*, and *L*1) are carefully designed. Also, the battery charging power can be determined without measuring the battery current. The control block diagram of the first BBC set, as an example, is shown in Fig.7. The discharging/charging and power commands, *D*/*C* and *Pb*1, are generated by the BMS and are sent to the controller of the BSG-inverter. The duty cycle signals, *Dp*1 and *dc*1, can be determined by using the derived (8) and (11). For the battery discharging operation, the unity sinusoidal function with the grid frequency, *sinωt*, can be via a phase-locked loop and is used to obtain the reference signal *Dp*1sin*ωt*. The gate signal of *Sd*1 can be generated by comparing *Dp*1sin*ωt* with the saw-tooth carrier signal *V*sw. Also, the gate signal of *Sc*1 can be generated by comparing the duty cycle *dc*1 with the saw-tooth carrier signal *V*sw for the battery charging operation.

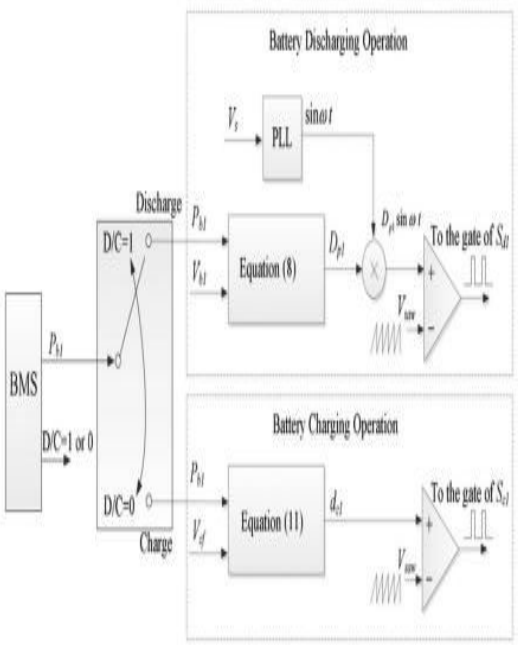

Fig.7. Control block diagram of the first BBC set.

The dc–ac unfolder is realized by four active switches operated at low switching frequency and an *LC* filter. It can convert the high frequency pulsating dc current generated by the BBCs into a sinusoidal one with utility line frequency. During the positive half-cycle of the ac mains, the switches *SA* and *SD* are turned-on while *SB* and *SC* are off. For the negative half-cycle, switches *SB* and *SC* are ON and *SA* and *SD* are OFF. Since the unfolder is switched at the ac line frequency, its switching loss is very low and can be neglected. Therefore, the proposed BSG-inverter only has one high-frequency PWM

International Journal for Innovative Engineering and Management Research
PEER REVIEWED OPEN ACCESS INTERNATIONAL JOURNAL
www.ijiemr.org

signal and can be categorized as a single-stage inverter. For the proposed BSG-inverter, the *m*-sets of BBCs can operate in the interleaving fashion. The required synchronization signal for the interleaving operation can be easily obtained from the ac line voltage and no extra communication between BBC is required. By shifting the duty cycles of adjacent channels with 360°/m, the total current ripple of the output inductor can be greatly reduced. Fig.3.8 shows the voltage and current waveforms of the BBC's output of two phase interleaving in battery discharging mode. The shifting time *Tm* of *m*-sets of BBCs can be expresses as follows:

$$T_m = \frac{1}{mf_s}. \tag{12}$$

Since the average voltage of output inductor *Lf* is zero at steady state, the average voltage across *Cf* is equal to *V*ac and the peak discharging time *T*off can be expressed as follows:

$$T_{\text{off}} = \frac{V_{b1} D_{p1}}{\sqrt{2} V_{\text{ac}} f_s}. \tag{13}$$

The discharging time of the capacitor *Cf* can be expressed as follows:

$$T_d = T_m - T_{\text{off}} = \frac{1}{mf_s} - \frac{V_{b1} D_{p1}}{\sqrt{2} V_s f_s}. \tag{14}$$

The peak voltage deviation of the output capacitor can be derived as follows:

$$\Delta V_{C_f} = \frac{T_d I_{\text{ac}}}{C_f} \tag{15}$$

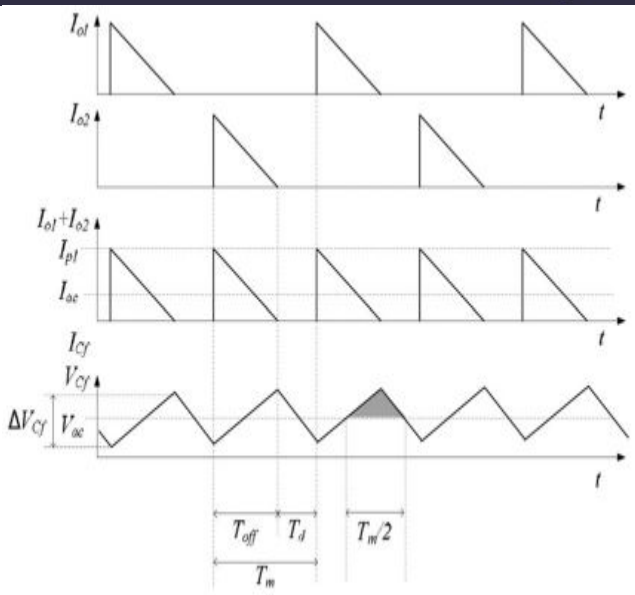

Fig.8. Output voltage and current waveforms of the BBC of two phase interleaving in battery discharging mode.

where *Cf* is the capacitor value and *I*ac is the peak value of the output current. Since the variation of the storage energy of the output capacitor is almost equal to the variation of the storage energy of the output inductor in *Tm* interval, the equation for the storage energy can be derived as follows:

$$E_d = \frac{1}{2} C_f \Delta V_{C_f}^2 = \frac{1}{2} L_f \Delta I_f^2 \tag{16}$$

where *Lf* is the output inductor value and Δ*If* is the peak current deviation of the output inductor. From (14)–(16), and Fig.8, the peak current deviation of the output inductor can be obtained as follows:

$$\Delta I_f = \sqrt{\frac{\left(\frac{1}{mf_s} - \frac{V_{b1} D_{p1}}{\sqrt{2} V_s f_s}\right)^2 I_{\text{ac}}^2}{L_f C_f}}. \tag{17}$$

Fig.9 shows the voltage and current waveforms of the BBC's output of two phases interleaving in charging mode. The average voltage across *Cf* must equal to *V*ac and the charging time *T*on can be expressed as follows:

International Journal for Innovative Engineering and Management Research
PEER REVIEWED OPEN ACCESS INTERNATIONAL JOURNAL
www.ijiemr.org

$$T_{on} = \frac{d_{c1}}{f_s}. \quad (18)$$

The charging time of the capacitor *Cf* can be expressed as follows:

$$T_c = T_m - T_{on} = \frac{1}{mf_s} - \frac{d_{c1}}{f_s}. \quad (19)$$

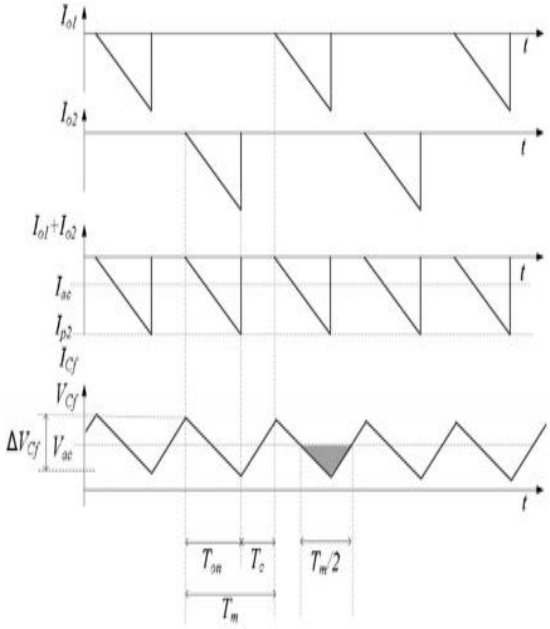

Fig.9. Output voltage and current waveforms of the BBC of two phase interleaving in battery charging mode.

The peak deviation of the output capacitor can be derived as follows:

$$\Delta V_{C_f} = \frac{T_c I_{ac}}{C_f}. \quad (20)$$

From (16), (19), (20), and Fig.3.8, the peak current deviation of the output inductor can be obtained as follows:

$$\Delta I_f = \sqrt{\frac{\left(\frac{1}{mf_s} - \frac{d_{c1}}{f_s}\right)^2 I_{ac}^2}{L_f C_f}}. \quad (21)$$

From (17) and (21), it can be found that the ripple current can be decreased by adding the numbers of the BBCs directly. This interleaved operation can result in lower ripple current to reduce the size of the output inductor and capacitor. Finally, the design procedure of the proposed BSG-inverter can be summarized as follows.

1) To ensure the DCM operation of the BBC, determine an eligible maximum duty ratio shown in (4) and (10) according to the rated voltage of the battery module and the ac mains.

2) Select the appropriate switching frequency and determine the total switching numbers shown in (1) with grid frequency.

3) Design the input inductor *L*1 shown in (8) and (11) with the circuit parameters *f*, *fs*, *Dp*1, *dc*1, *N*, and *Pb*1.

4) Based on the numbers of battery modules, shift the duty cycles of adjacent channels with 360°/m for the interleaving operation.

5) Select the appropriate value of the output current ripple to determine the output inductor and capacitor shown in (17) and (21) with the circuit parameters *m*, *Tm* , *Lp*1, *L*1, *Vs*, and *I*ac.

III. MULTILEVEL INVERTERS

In the industries, the applications like mills, laminators, conveyors, fans and pumps etc require high power and medium voltage. Such a high power applications the multilevel inverter (MLI) topology is extending the usage because of its own advantages. The conventional square wave inverter produces more harmonics and in multilevel inverter the output voltage wave shape is nearly sinusoidal with number of levels. The advantages of multilevel inverter are listed below.

1. The stress of the motor is reduced and protects the motor against damage.
2. Multilevel inverters draw the current from source with less distortion.
3. These can operate at high as well as lower frequencies.

International Journal for Innovative Engineering and Management Research
PEER REVIEWED OPEN ACCESS INTERNATIONAL JOURNAL
www.ijiemr.org

4. The total harmonic distortion (THD) is less in the output voltage wave form without using any filter.

Owing to these advantages different types of multilevel inverters are introduced in to the market such as diode clamped type, flying capacitor type and cascaded multilevel inverter.

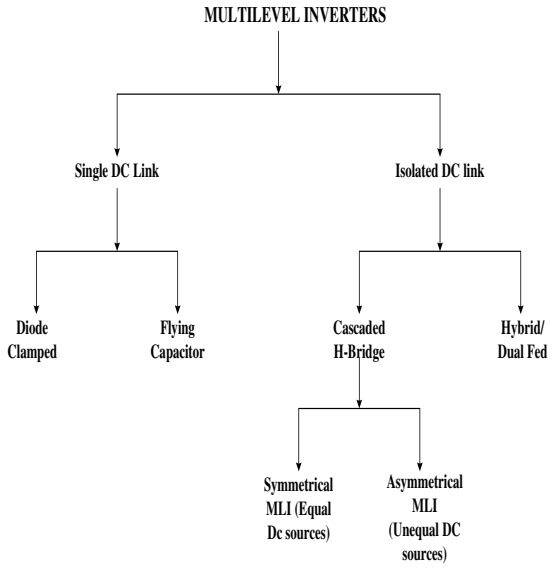

Fig.10. Classification of Multilevel Inverters

IV. INDUCTION MOTOR

An induction motor is an example of asynchronous AC machine, which consists of a stator and a rotor. This motor is widely used because of its strong features and reasonable cost. A sinusoidal voltage is applied to the stator, in the induction motor, which results in an induced electromagnetic field. A current in the rotor is induced due to this field, which creates another field that tries to align with the stator field, causing the rotor to spin. A slip is created between these fields, when a load is applied to the motor. Compared to the synchronous speed, the rotor speed decreases, at higher slip values. The frequency of the stator voltage controls the synchronous speed. The frequency of the voltage is applied to the stator through power electronic devices, which allows the control of the speed of the motor. The research is using techniques, which implement a constant voltage to frequency ratio. Finally, the torque begins to fall when the motor reaches the synchronous speed. Thus, induction motor synchronous speed is defined by following equation,

$$n_s = \frac{120 f}{P}$$

Where f is the frequency of AC supply, n, is the speed of rotor; p is the number of poles per phase of the motor. By varying the frequency of control circuit through AC supply, the rotor speed will change.

V. MATLAB/SIMULINK RESULTS

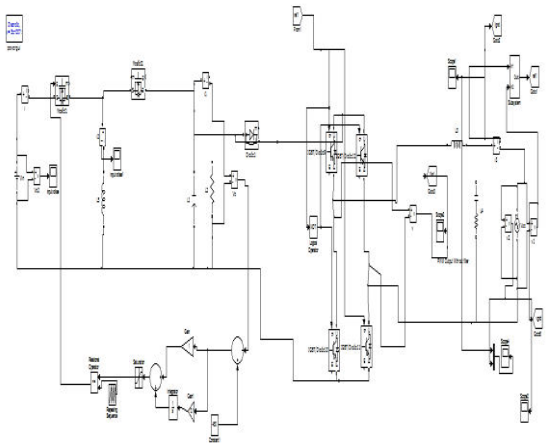

Fig.11 Matlab/simulink Model of Proposed BSG-Inverter with Battery Discharging Mode

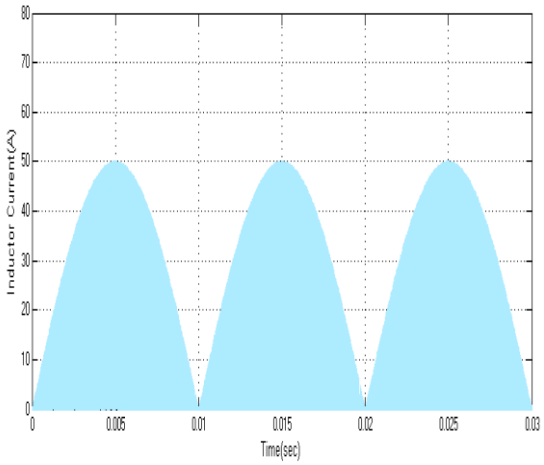

Fig.12 Inductor current in Discharging mode

International Journal for Innovative Engineering and Management Research
PEER REVIEWED OPEN ACCESS INTERNATIONAL JOURNAL
www.ijiemr.org

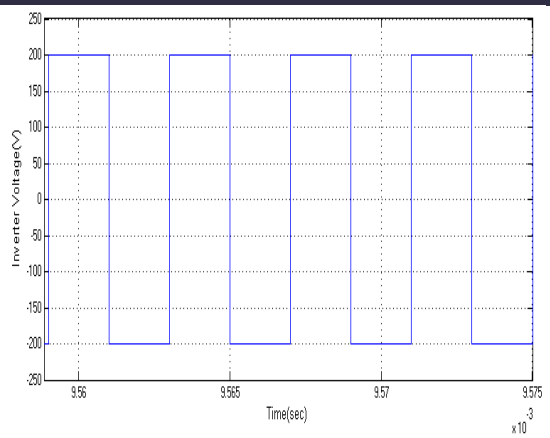

Fig.13 Inverter Voltage in Battery Discharging mode

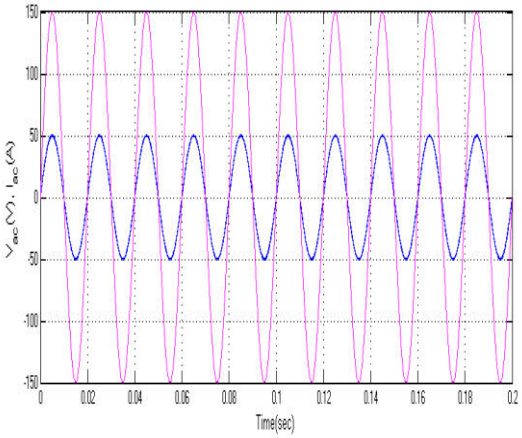

Fig.14 Ac main Voltage and Output current for BSG-Inverter in Discharging mode

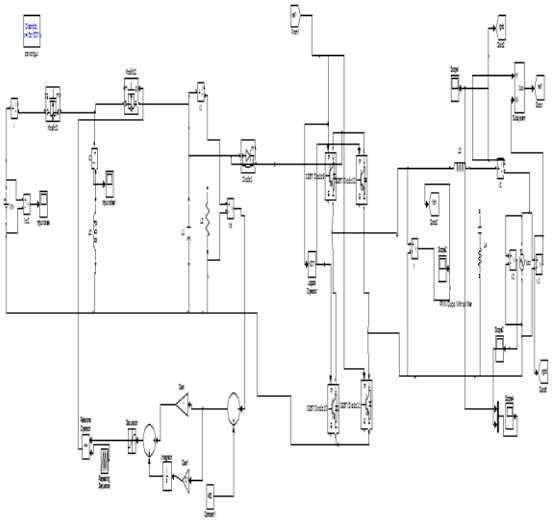

Fig.14 Matlab/simulink Model of Proposed BSG-Inverter with Battery charging Mode

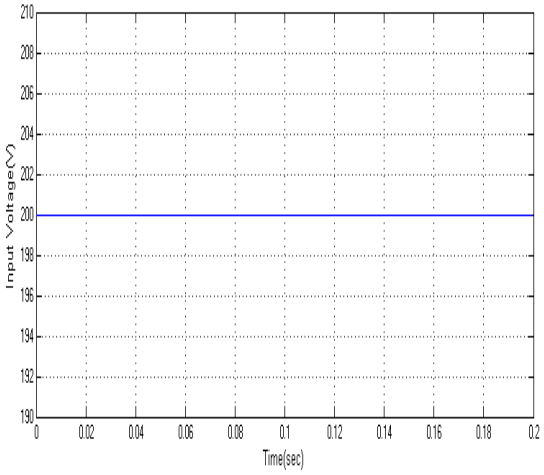

Fig.15 Input Voltage

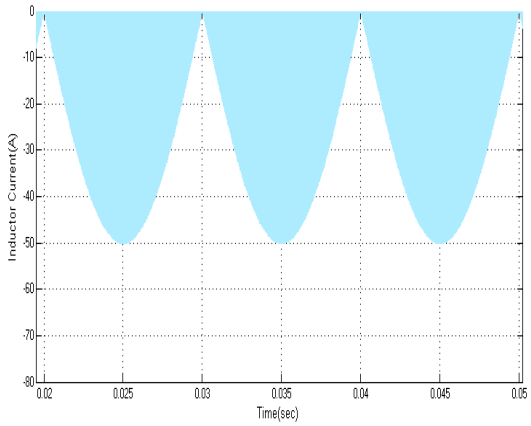

Fig.16 Inductor current in charging mode

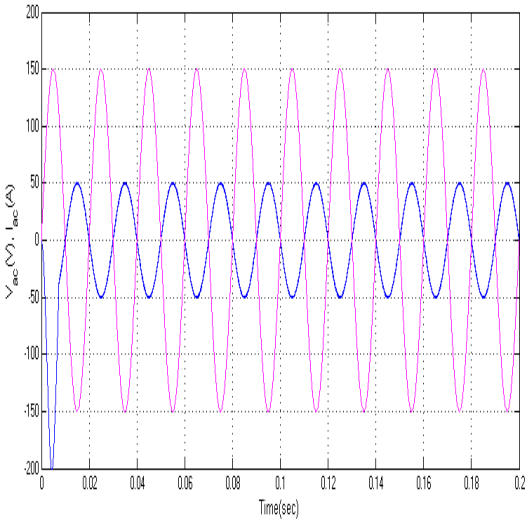

Fig.17 Ac main Voltage and Output current for BSG-Inverter in charging mode

International Journal for Innovative Engineering and Management Research
PEER REVIEWED OPEN ACCESS INTERNATIONAL JOURNAL
www.ijiemr.org

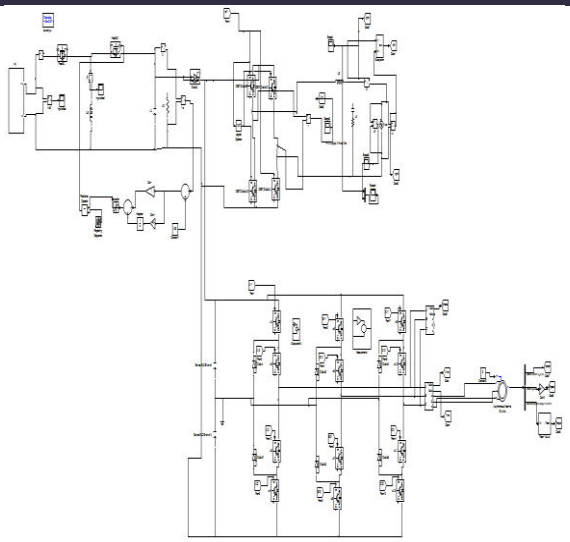

Fig.18 Matlab/simulink model of Proposed BSG-Inverter with PV fed Induction Motor

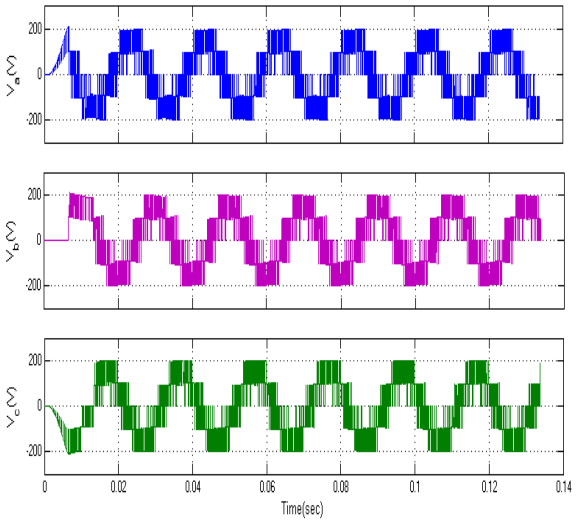

Fig.19 Line-Line Voltages of MLI

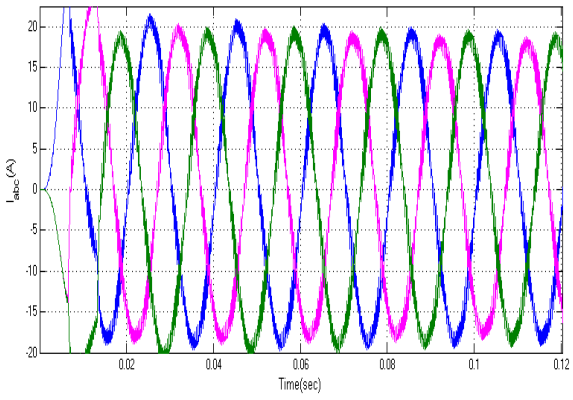

Fig.20 output Currents

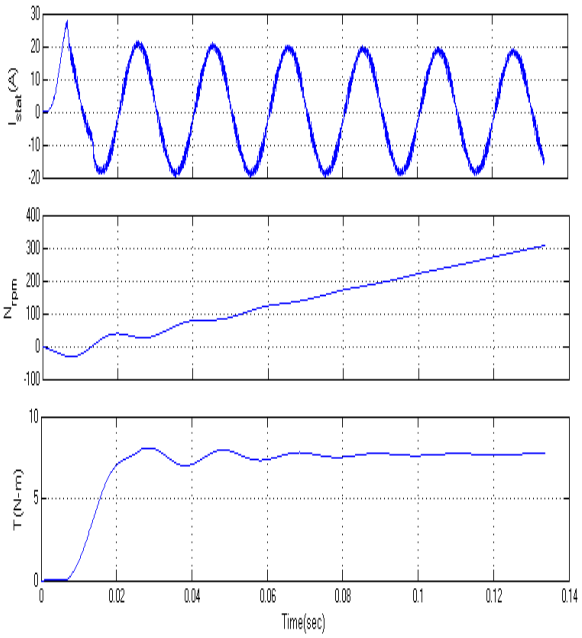

Fig.21 Stator currents, Speed and Torque of Induction machine

6. CONCLUSION

A novel BSG-inverter, which consists of multiple distributed BBCs and a dc–ac unfolder, for the battery energy storage system has been proposed in this paper. The proposed BSG-inverter has individual power control capability for each battery module while fulfills the functions of battery charging and discharging by using pulsating current. Eventually, the equalization, lifetime extension, and capacity flexibility of the battery energy storage system can be achieved. According to the developed mathematical equations, the power control capability of each individual battery module can be achieved without the need of input current sensor. Also, with the interleaved operation, the current ripple of the output inductor can be reduced significantly. A design guide line of the proposed BSG is presented. Finally, solar power fed Proposed BSG Inverter for Industrial applications with MLI is designed in Matlab/simulink software and the simulation measurements are shown to verify the validity of the proposed BSG-inverter.

REFERENCES

[1] J. Y. Kim, J. H. Jeon, S. K. Kim, C. Cho, J. H. Park, H.-M. Kim, and K. Y. Nam, "Cooperative control strategy of energy storage system and micro sources for stabilizing the microgrid during islanded operation," *IEEE Trans. Power Electron.*, vol. 25, no. 12, pp. 3037–3048, Dec. 2010.

[2] H. Qian, J. Zhang, J. S. Lai, and W. Yu, "A high-efficiency grid-tie battery energy storage system," *IEEE Trans. Power Electron.*, vol. 26, no. 3, pp. 886–896, Mar. 2011.

[3] J. He and Y. W. Li, "Hybrid voltage and current control approach for DG grid interfacing converters with LCL filters," *IEEE Trans. Ind. Electron.*, vol. 60, no. 5, pp. 1797–1809, Mar. 2013.

[4] M. Y. Kim, C. H. Kim, J. H. Kim, and G. W. Moon, "A chain structure of switched capacitor for improved cell balancing speed of lithium-ion batteries," *IEEE Trans. Ind. Electron.*, vol. 61, no. 8, pp. 3989–3999, Aug. 2014.

[5] K. M. Lee, Y. H. Chung, C. H. Sung, and B. Kang, "Active cell balancing of Li-ion batteries using LC series resonant circuit," *IEEE Trans. Ind. Electron.*, vol. 62, no. 9, pp. 5491–5501, Sep. 2015.

[6] W. Huang and A. Qahouq, "Energy sharing control scheme for state of-charge balancing of distributed battery energy storage system," *IEEE Trans. Ind. Electron.*, vol. 62, no. 5, pp. 2764–2776, May 2015.

[7] C. L. Chen, Y. Wang, J. S. Lai, and Y. S. Lee, "Design of parallel inverters for smooth mode transfer microgrid applications," *IEEE Trans. Power Electron.*, vol. 25, no. 1, pp. 6–14, Jan. 2010.

[8] N. Mukherjee and D. Strickland, "Control of second-life hybrid battery energy storage system based on modular boost multilevel buck converter," *IEEE Trans. Ind. Electron.*, vol. 62, no. 2, pp. 1034–1046, Feb. 2015.

[9] H. Hu, S. Harb, N. H. Kutkt, Z. J. Shen, and I. Batarseh, "A single-stage micro inverter without using electrolytic capacitors," *IEEE Trans. Power Electron.*, vol. 28, no. 6, pp. 2677–2687, Jun. 2013.

[10] N. Sukesh, M. Pahlevaninezhad, and P. K. Jain, "Analysis and implementation of a single-stage fly back PV micro inverter with soft switching," *IEEE Trans. Ind. Electron.*, vol. 61, no. 4, pp. 1819–1833, Apr. 2014.

[11] W. J. Cha, Y. W. Cho, and B. H. Kwon, "Highly efficient micro inverter with soft-switching step-up converter and single-switch-modulation inverter," *IEEE Trans. Ind. Electron.*, vol. 62, no. 6, pp. 3516–3523, Jun. 2015.

[12] L. Maharjan, T. Yamagishi, and H. Akagi, "Active-power control of individual converter cells for a battery energy storage system based on a multilevel cascade PWM converter," *IEEE Trans. Power Electron.*, vol. 27, no. 3, pp. 1099–1107, Mar. 2012.

[13] M. Vasiladiotis and A. Rufer, "A modular multiport power electronic transformer with integrated split battery energy storage for versatile ultrafast EV charging stations," *IEEE Trans. Ind. Electron.*, vol. 62, no. 5, pp. 3213–3222, May 2015.

[14] L. R. Chen, J. J. Chen, C. M. Ho, S. L. Wu, and D. T. Shieh, "Improvement of Li-ion battery discharging performance by pulse and sinusoidal current strategies," *IEEE Trans. Ind. Electron.*, vol. 60, no. 12, pp. 5620–5628, Dec. 2013.

[15] L. R. Chen, S. L. Wu, D. T. Shieh, and T. R. Chen, "Sinusoidal-ripple current charging strategy and optimal charging frequency study for Li-ion batteries," *IEEE Trans. Ind. Electron.*, vol. 60, no. 1, pp. 88–97, Jan. 2013.

[16] J. Li, E. Murphy, J. Winnick, and P. A. Kohl, "The effects of pulse charging on cycling characteristics of commercial lithium-ion batteries," *J. Power Sources*, vol. 102, pp. 302–309, 2001.

[17] M. Liserre, F. Blaabjerg, and S. Hansen, "Design and control of an LCLfilter-based three-phase active rectifier," *IEEE Trans. Ind. Appl.*, vol. 41, no. 5, pp. 1281–1291, Sep./Oct. 2005.

[18] S. B. Kjaer, J. H. Pedersen, and F. Blaabjerg, "A review of single phase grid-connected inverters for photovoltaic modules," *IEEE Trans. Ind. Appl.*, vol. 41, no. 5, pp. 1292–1306, Sep. 2005.

[19] E. Koutroulis and F. Blaabjerg, "Design optimization of transformerless grid-connected PV inverters including reliability," *IEEE Trans. Power Electron.*, vol. 28, no. 1, pp. 325–335, Jan. 2013.

[20] E. S. Sreeraj, K. Chatterjee, and S. Bandyopadhyay, "One-cycle-controlled single-stage single-phase voltage-sensor less grid-connected PV system," *IEEE Trans. Ind. Electron.*, vol. 60, no. 3, pp. 1216–1224, Mar. 2013.